C. elegans bicd-1, homolog of the Drosophila dynein accessory factor Bicaudal D, regulates the branching of PVD sensory neuron dendrites

Cristina Aguirre-Chen[1], Hannes E. Bülow[1,2] and Zaven Kaprielian[1,3,*]

SUMMARY

The establishment of cell type-specific dendritic arborization patterns is a key phase in the assembly of neuronal circuitry that facilitates the integration and processing of synaptic and sensory input. Although studies in *Drosophila* and vertebrate systems have identified a variety of factors that regulate dendrite branch formation, the molecular mechanisms that control this process remain poorly defined. Here, we introduce the use of the *Caenorhabditis elegans* PVD neurons, a pair of putative nociceptors that elaborate complex dendritic arbors, as a tractable model for conducting high-throughput RNAi screens aimed at identifying key regulators of dendritic branch formation. By carrying out two separate RNAi screens, a small-scale candidate-based screen and a large-scale screen of the ~3000 genes on chromosome IV, we retrieved 11 genes that either promote or suppress the formation of PVD-associated dendrites. We present a detailed functional characterization of one of the genes, *bicd-1*, which encodes a microtubule-associated protein previously shown to modulate the transport of mRNAs and organelles in a variety of organisms. Specifically, we describe a novel role for *bicd-1* in regulating dendrite branch formation and show that *bicd-1* is likely to be expressed, and primarily required, in PVD neurons to control dendritic branching. We also present evidence that *bicd-1* operates in a conserved pathway with *dhc-1* and *unc-116*, components of the dynein minus-end-directed and kinesin-1 plus-end-directed microtubule-based motor complexes, respectively, and interacts genetically with the repulsive guidance receptor *unc-5*.

KEY WORDS: PVD, Dendrite morphogenesis, Bicaudal D, *Caenorhabditis elegans*

INTRODUCTION

Dendrites receive and process synaptic and sensory inputs via elaborate dendritic networks or arbors. Although the complexity and shape of these networks vary widely among different neuronal subtypes, a given class of neuron displays highly stereotyped dendritic arbors (Grueber et al., 2005). Accordingly, cell type-specific dendritic arborization patterns help to define the specific inputs and functional outputs associated with a given neuronal subtype (Hausser et al., 2000). Dendritic branching represents a key step(s) in the formation of dendritic arbors. Whereas studies in *Drosophila* and vertebrate systems have identified a variety of molecules that regulate dendrite branching (Corty et al., 2009; Jan and Jan, 2010; Urbanska et al., 2008), the full repertoire of molecules controlling this crucial stage of dendrite development remains obscure.

RNA interference (RNAi) is a well-established powerful tool for identifying novel genes involved in a wide range of biological phenomena (Fire et al., 1998; Wolters and MacKeigan, 2008). In *C. elegans*, large-scale RNAi screens have been used to define key sets of genes involved in processes such as fat regulation (Ashrafi et al., 2003), longevity (Hamilton et al., 2005) and axon guidance (Schmitz et al., 2007). Therefore, we reasoned that RNAi screens in *C. elegans* might uncover novel regulators of dendritic

branching. Specifically, we chose to carry out RNAi screens to identify genes that regulate the branching of PVD neuron dendrites in *C. elegans*. PVD neurons are bilaterally symmetric nociceptors that respond to harsh mechanical stimuli and cold temperatures (Chatzigeorgiou et al., 2010; Way and Chalfie, 1989). Importantly, these neurons elaborate large and complex dendritic arbors which envelop the body of late-larval and adult-staged animals (Oren-Suissa et al., 2010; Smith et al., 2010; Tsalik et al., 2003; Yassin et al., 2001), and provide an ideal system for studies aimed at identifying novel regulators of dendrite morphogenesis.

To date, *mec-3*, which encodes a LIM homeodomain transcription factor expressed in PVD neurons (Way and Chalfie, 1988; Way and Chalfie, 1989), as well as *eff-1*, which encodes a protein essential for cell fusion, are the only genes known to be required for the elaboration of PVD dendritic arbors (Oren-Suissa et al., 2010; Tsalik et al., 2003). By carrying out two RNAi screens, a small-scale candidate-based screen and a large-scale screen of chromosome IV, we identified 11 genes that either promote or suppress PVD dendrite branching. These include: *bicd-1*, homologs of which include *Drosophila Bicaudal D* (*BicD*) (Suter et al., 1989; Wharton and Struhl, 1989) and mammalian *bicaudal D homolog 1* (*BICD1*) and *bicaudal D homolog 2* (*BICD2*) (Baens and Marynen, 1997; Hoogenraad et al., 2001); *dnc-1* and *dli-1*, which encode components of the cytoplasmic dynein minus-end-directed motor (Koushika et al., 2004); and *unc-116*, which encodes a component of the kinesin-1 plus-end-directed motor (Patel et al., 1993; Sakamoto et al., 2005). *Drosophila* BicD facilitates the localization and transport of mRNAs (Bullock and Ish-Horowicz, 2001; Bullock et al., 2006) and nuclei (Swan et al., 1999) via interactions with Dynein, and mammalian BICD1 and BICD2 co-precipitate with dynein and dynactin and function in dynein-mediated

[1]Dominick P. Purpura Department of Neuroscience, Albert Einstein College of Medicine, Bronx, NY 10461, USA. [2]Department of Genetics, Albert Einstein College of Medicine, Bronx, NY 10461, USA. [3]Department of Pathology, Albert Einstein College of Medicine, Bronx, NY 10461, USA.

*Author for correspondence (Zaven.Kaprielian@einstein.yu.edu)

transport (Hoogenraad et al., 2001; Hoogenraad et al., 2003; Matanis et al., 2002). Given that a function for *bicd-1* in dendritic branch formation had not been established, and the connections between *bicd-1* and microtubule-based motors in other systems, we investigated the role of *bicd-1* and the motor components retrieved from our screens in PVD dendrite branching.

Here, we demonstrate that loss of *bicd-1* function results in the appearance of ectopic dendrite branches posterior and proximal to the PVD cell body with a concomitant reduction in the number of terminal branches elaborated distal to the PVD cell body. In addition, our *bicd-1::*YFP transcriptional reporter data, coupled with anatomical focus-of-action studies, indicate that *bicd-1* is expressed, and primarily acts, in PVD neurons. Furthermore, we show that *bicd-1* acts cooperatively with both *dhc-1* and *unc-116* to regulate PVD dendrite branching. Interestingly, our RNAi screens also identified *unc-5*, a known repulsive guidance receptor (Leung-Hagesteijn et al., 1992), as a regulator of PVD dendritogenesis and we present evidence that *bicd-1* interacts genetically with *unc-5* in this context. Together, these findings identify *bicd-1* as a key regulator of dendrite branching in *C. elegans* and suggest novel mechanisms, crucial for proper dendrite morphogenesis, that may be conserved in higher-order organisms.

MATERIALS AND METHODS
Strains
C. elegans strains were maintained on nematode growth media plates at 20°C (unless otherwise noted) using standard techniques (Brenner, 1974). The wild-type strain is N2 Bristol. The PVD transcriptional reporter is OH1422 [*otIs138* (*ser2prom3::GFP*) X] (Tsalik et al., 2003) and the FLP transcriptional reporter is NY2030 [*ynIs30* (*Pflp4::GFP*) I] (Kim and Li, 2004). All mutant strains were provided by the *Caenorhabditis* Genetics Center. The temperature sensitive *dhc-1(or195)* mutants were maintained at 15°C and shifted to the restrictive temperature of 25°C for phenotypic analysis. *bicd-1* is the gene name for *C43G2.2* and is used throughout this study.

Strain construction
RZ117 [*bicd-1(ok2731);otIs138*], RZ119 [*dhc-1(or195);otIs138*], RZ120 [*unc-116(e2310);otIs138*], RZ121 [*unc-5(e152);otIs138*], RZ155 [*unc-5(e53);otIs138*], RZ134 [*unc-6(ev400) otIs138*], RZ131 [*bicd-1(ok2731);ynIs30*], RZ136 [*dhc-1(or195);bicd-1(ok2731);otIs138*], RZ103 [*unc-116(e2310);bicd-1(ok2731);otIs138*], RZ135 [*unc-5(e152) bicd-1(ok2731);otIs138*], RZ157 [*unc-5(e53) bicd-1(ok2731);otIs138*] and RZ165 [*bicd-1(ok2731);unc-6(ev400) otIs138*] were generated using standard techniques. *bicd-1(ok2731)* animals were backcrossed three times to N2 (wild type) prior to strain construction. Primers used to identify *bicd-*

1(ok2731) IV mutant animals were (5′-3′): CATTAACATCTGTC-TCTGTTCCAC, CATACATCTACGCTAGACTCC and GCAAGTGACC-TCTTCAGTGAATTAC. Primers used to identify *bicd-1(tm3421)* IV mutant animals were (5′-3′):   GAATGCTTGTTCAGAGGTTC, CACATCGCCAATCTTGACAC and TCAGGACGCAATGATTCAAG.

RNAi screening
RNAi by feeding was performed as previously described (Kamath and Ahringer, 2003; Schmitz et al., 2007) with minor modifications. Briefly, RNAi clones were grown for 16 hours in LB media with 50 μg/ml ampicillin. Bacterial cultures were seeded onto agar plates containing 1 mM isopropyl β-D-1-thiogalactopyranoside (IPTG) (Sigma) and 50 μg/ml carbenicillin and allowed to dry for 24 to 48 hours at room temperature. Three L4 larval stage hermaphrodites were then placed on each plate, incubated for 4 days at 20°C and allowed to lay a brood. After incubation, young adult progeny were washed off feeding pates with M9 buffer and mounted on 5% agar pads. Approximately twenty adult progeny per RNAi clone were scored for the presence of defective PVD dendritic morphology, defined here as a qualitative increase or decrease in the number of secondary, tertiary or quaternary dendrites. All RNAi clones (kindly provided by Ji Y. Sze, Albert Einstein College of Medicine of Yeshiva University, NY, USA) assayed in the candidate-based screen were tested twice and subjected to at least two additional rounds of re-testing if ≥10% of animals displayed defective PVD morphology in either initial test. RNAi clones (Geneservice) (Fraser et al., 2000; Kamath et al., 2003) assayed in the large-scale screen were re-tested at least twice if ≥18% of animals displayed a defective PVD arborization pattern. Data from all RNAi tests (three to five tests per RNAi clone) were then pooled to generate an overall percentage of animals displaying defects. RNAi clones were considered positive if the overall percentage of animals displaying a defective PVD arborization pattern was ≥20% (Table 1). Note that RNAi against either *dnc-1* or *unc-32* produced very few animals that survived to adulthood. Therefore, it was not possible to assay the targeted twenty animals per test for these genes. Additionally, 335 (candidate screen: 7; chromosome IV screen: 328) of the 2830 total RNAi clones (candidate screen: 137; chromosome IV screen: 2693) were not assessed owing to technical difficulties (e.g. clone failed to grow, mold/bacterial contamination of seeded clone). All inserts from positive RNAi clones were sequenced to confirm their identities.

Plasmid construction and transgenic strains
The *bicd-1::*YFP fusion construct was generated by PCR fusion (Hobert, 2002). Specifically, a 5977 bp fragment upstream of the ATG start codon of *bicd-1* was amplified from N2 worm genomic DNA and fused to the *yfp/unc-54* 3′UTR cassette. *bicd-1::*YFP was injected into N2 wild-type animals at 25 ng/μl, using pRF4 *rol-6(su1006)* as an injection marker.

For cosmid rescue experiments, the C43G2 cosmid (2 ng/μl) was injected with *mec-7::gfp* and *myo-3::rfp* plasmids (50 ng/μl each). For cell type-specific rescue experiments, *bicd-1* cDNA was PCR amplified from

Table 1. Candidate-based and large-scale RNAi screens identify genes required for the proper branching of PVD dendrites

Gene	Description	RNAi phenotype	Animals defective (%)	n
unc-86	POU-homeodomain transcription factor	Decrease in number of secondary, tertiary and quaternary branches	38	69
unc-116	Kinesin-1 heavy chain	Decrease in number of secondary, tertiary and quaternary branches	45	65
gex-2	p140/Sra1	Decrease in number of quaternary branches	26	106
unc-115	Actin-binding LIM Zn-finger protein	Decrease in number of quaternary branches	76	58
unc-44	Ankyrin	Decrease in number of quaternary branches	20	115
unc-70	Beta-spectrin	Decrease in number of quaternary branches	49	55
bicd-1	Bicaudal-D	Increase in number of tertiary branches	61	72
dnc-1	Dynactin	Increase in number of tertiary branches	94	33
dli-1	Dynein light intermediate chain	Increase in number of tertiary branches	69	55
unc-32	Vacuolar H+-ATPase V0 sector, subunit a	Increase in number of tertiary branches	45	20
F46F11.9	GSG1	Increase in number of tertiary branches	27	90

A total of 11 genes that are required for the branching of PVD dendrites were retrieved from both RNAi screens: *bicd-1*, *dnc-1*, *dli-1*, *unc-44* and *gex-2* from the large-scale screen, and *unc-86*, *unc-116*, *unc-115*, *unc-70*, *unc-32* and *F46F11.9* from the candidate-based screen. Animals were scored as defective if they exhibited a conspicuous increase or decrease in the number of secondary, tertiary or quaternary PVD dendrite branches.
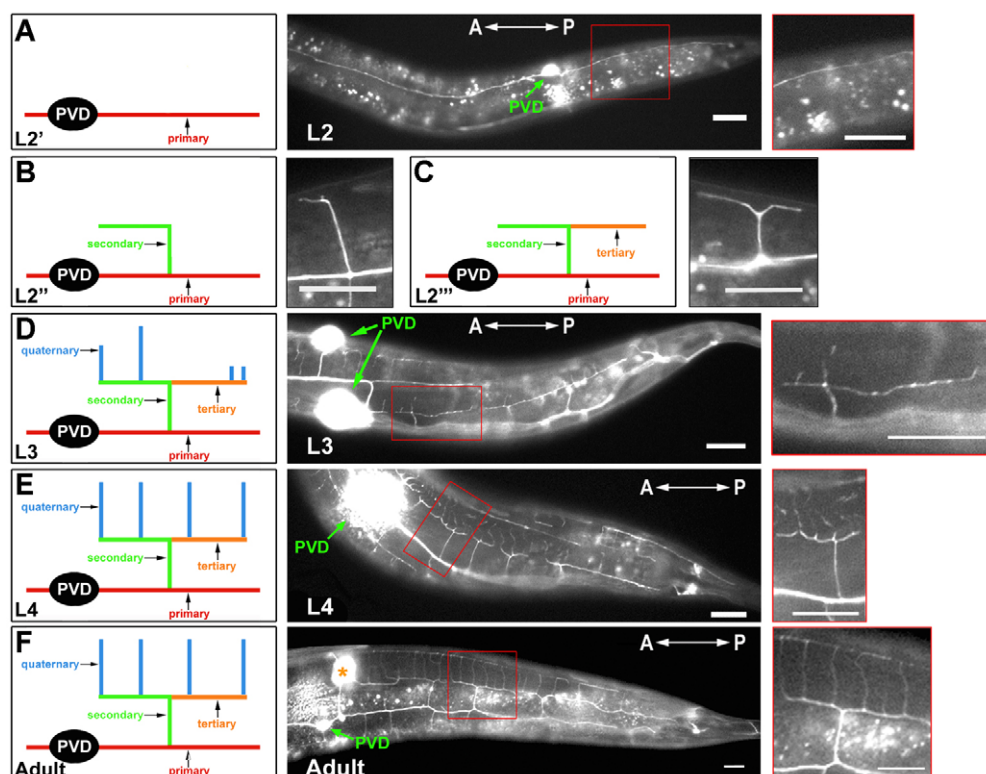
Fig. 1. Spatiotemporal pattern of PVD dendrite branching. (**A-F**) The *otIs138* transcriptional reporter was used to characterize the branching of PVD dendrites in the tail region, posterior to the PVD cell body, of wild-type worms at the L2 (A-C; L2′, L2″ and L2‴ refer to progressively later stages of development in L2 animals), L3 (D) and L4 (E) larval stages and at the young adult stage (F). Schematic representations of reporter labeling of PVD dendritic arbors are shown together with low (A,D-F) and high (A-F) magnification images of examples of the schematized projections. Red boxes in A and D-F represent the area shown in the high magnification image. Anteroposterior orientation is indicated by the white double-headed arrow. Asterisk in F denotes the spermatheca. The labeling of only one (left or right) PVD neuron and one of its dendritic trees is depicted in each schematic, and labeled PVD neuron cell bodies are identified by arrows in each of the middle panels. Scale bars: 10 μm.

the *C. elegans* ORFeome clone OCE1182-7243564 (Open Biosystems) and cloned into pPD96.41, creating pZK01. After cloning the *bicd-1* cDNA into pPD96.41, the QuikChange Lightning Multi Site-Directed Mutagenesis System (Stratagene) was used to replace two nucleotides, C2646T and T3248C, which did not coincide with the predicted *bicd-1* nucleotide sequence. The *bicd-1* cDNA/*unc-54* 3′UTR cassette was then released from pZK01 and cloned into the pZK02 (*ser2prom3* promoter) and pPD95.86 (*myo-3* promoter) plasmids. Constructs were injected at 5ng/μl with *pceh-22::gfp* (pharyngeal GFP) and *pBS SK Bluescript* at 50 ng/μl each.

Quantification and photodocumentation of PVD dendrite branching defects
Unless otherwise noted, dendrite branching defects were scored at the young adult stage (52-58 hours post-hatch at 20°C or 42-44 hours post-hatch at 25°C). Dendrite branching defects were visualized with an Olympus IX 70 Microscope equipped with GFP and YFP optical filter sets (Chroma Technology). Images were captured with an Olympus Optronics digital camera and Magnafire 2.0 software.

Statistics
GraphPad Prism Software (Version 5.0b) was used for all statistical analyses.

RESULTS
Development of the PVD neuron dendritic arbor
The *otIs138* transcriptional reporter line (Tsalik et al., 2003) prominently labels the bilaterally symmetric PVD neurons and was used to characterize the development of PVD dendritic arbors from the L2 larval to the young adult stage. The primary anterior and posterior dendrites, which terminate posterior to the terminal bulb of the pharynx and at the endpoint of the tail, respectively, were clearly detectable by the L2 stage (Fig. 1A). Dorsally and ventrally directed secondary dendrites then grew out from the primary dendrites along the entire anteroposterior (A/P) axis of the animal

(Fig. 1B). Upon reaching the hypodermal/muscle border, secondary dendrites executed an orthogonal turn, in either the anterior or posterior direction, and extended parallel to the primary dendrite (Fig. 1B). Next, tertiary dendrites sprouted from the orthogonal turnpoint of existing secondary dendrites and, subsequently, projected longitudinally away from secondary dendrites (Fig. 1C). At L3, quaternary dendrites grew out from the longitudinally projecting segments of secondary and tertiary dendrites, and projected towards either the ventral or dorsal midline (Fig. 1D). Outgrowth of the quaternary dendrites was complete by the L4 stage (Fig. 1E) and the resulting arborization pattern was maintained at the young adult stage (Fig. 1F).

RNAi can effectively knock down gene expression in PVD neurons
Given that both cell-autonomous and non-cell-autonomous mechanisms are likely to control PVD dendrite development, it was imperative that our RNAi screens were capable of identifying genes that act in either PVD or the surrounding tissue (or both). To determine whether RNAi-mediated gene knockdown functions efficiently in PVD neurons, we attempted RNAi directly in the *otIs138* PVD reporter. We found that GFP expression in PVD neurons was markedly reduced in *otIs138* animals fed GFP dsRNA (Fig. 2A,B,D). Next, we fed *mec-3* dsRNA to *otIs138* animals, as *mec-3* encodes a LIM homeobox transcription factor that is expressed, and probably functions autonomously, in PVD (Way and Chalfie, 1988; Way and Chalfie, 1989) to regulate the branching of its dendrites (Tsalik et al., 2003). Of the 127 animals treated with a *mec-3* RNAi construct, 50% exhibited a reduced-branching phenotype similar to that displayed by *mec-3* genetic mutants (Fig. 2C,E). Together, these observations indicate that our RNAi approach can be used to identify genes that act autonomously in PVD neurons.
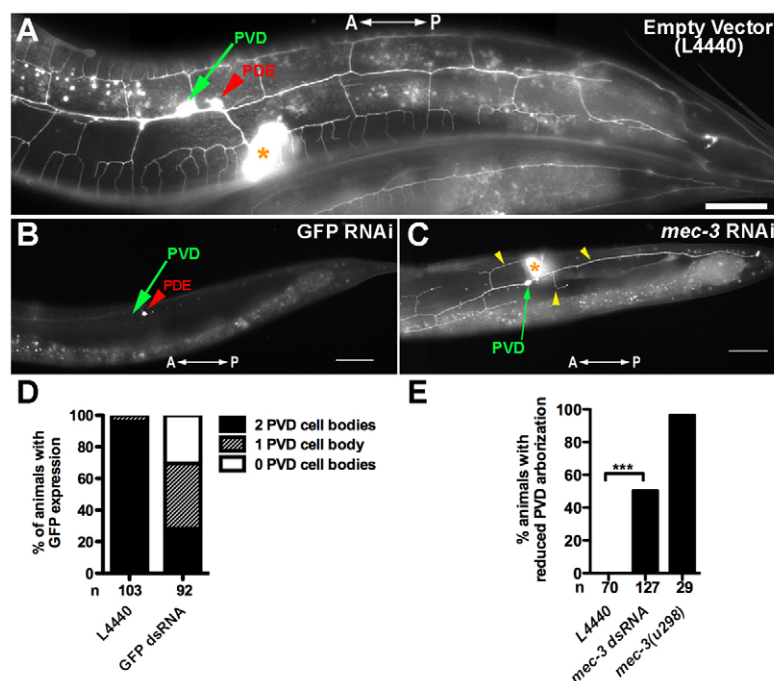
Fig. 2. RNAi constructs fed to wild-type worms efficiently knock down gene expression in PVD neurons. (**A,B,D**) *otIs138* animals fed the empty vector construct, L4440, display minimal knockdown of GFP protein expression in PVD neurons (A); 96% of animals retain GFP expression in both PVD cell bodies (D). The green and red arrows in A point to labeled PVD and PDE cell bodies, respectively. *otIs138* animals fed GFP dsRNA exhibit reduced GFP protein expression in PVD neurons (B); 28.3% of animals exhibit GFP expression in both PVD cell bodies, 41.3% express GFP in one PVD cell body only and 30.4% exhibit no GFP expression in both PVD cell bodies (D). The green arrow in B indicates the absence of GFP protein expression in a location presumably occupied by the PVD neuron. Because diminished GFP expression within PVD neurons prevented the visualization of PVD dendritic arbors (data not shown) in an RNAi hypersensitive strain (Schmitz et al., 2007), we conducted the complete screen in an otherwise wild-type background. (**C,E**) Half of *otIs138* animals fed *mec-3* dsRNA (C) display a significant reduction in the numbers of secondary, tertiary and quaternary dendrites (E), phenocopying the branch-reducing phenotype exhibited by *mec-3(u298)* genetic mutants. Anteroposterior orientation is indicated by the white double-headed arrow. The asterisks in A and C mark the spermatheca. Scale bars: 50 μm. Error bars represent s.e.m. ***P<0.001 determined by Fisher's exact test.
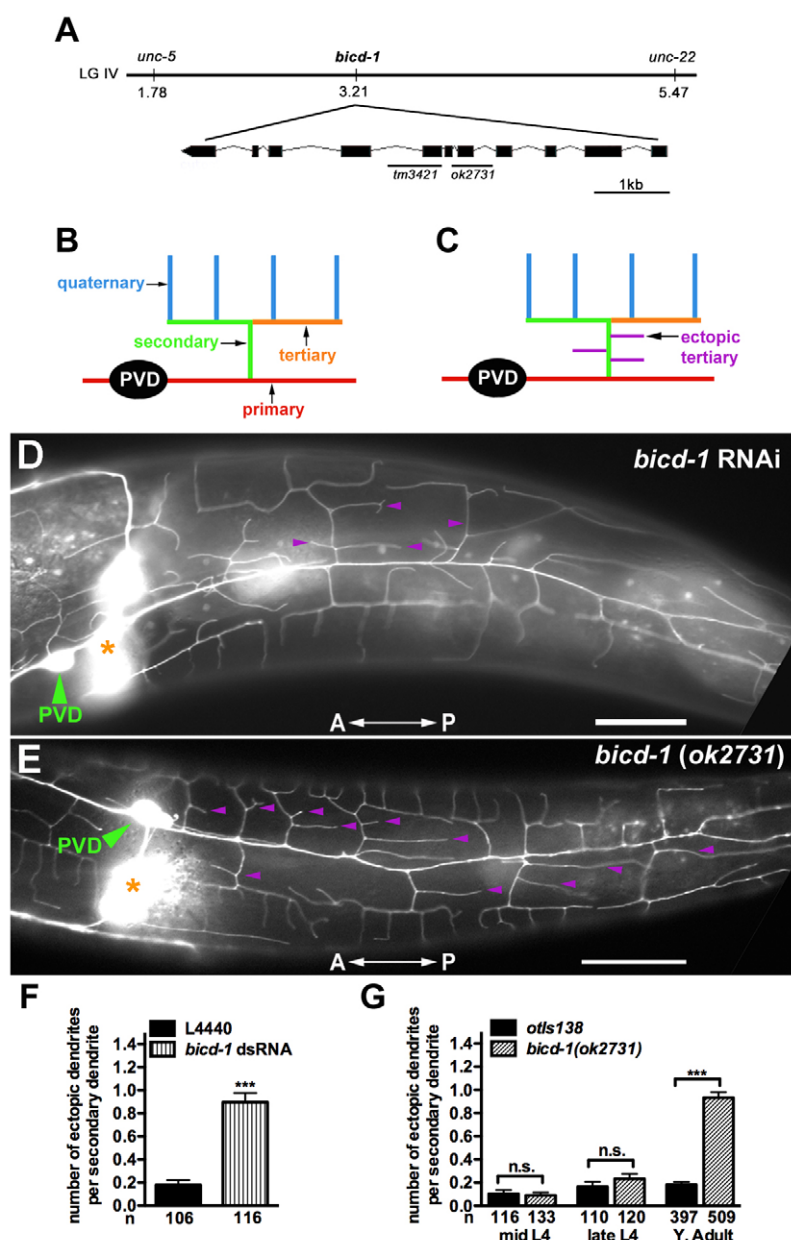
RNAi screens identify genes required for the formation of PVD dendritic arbors

To identify novel regulators of PVD dendrite development, we carried out both a small-scale candidate-based screen and a large-scale unbiased RNAi screen. In the candidate screen, we tested 121 genes known to regulate various aspects of neuronal development (Bülow et al., 2002; Kakimoto et al., 2006; Kim et al., 2007; Marshak et al., 2007; Miyashita et al., 2004; Schmitz et al., 2007; Struckhoff and Lundquist, 2003) or 16 PVD-specific genes (WormBase, release WS170, 02/09/07; see Table S1 in the supplementary material). In the large-scale screen, we individually knocked down 2693 genes on chromosome IV (Kamath et al., 2003). RNAi defects were categorized as either a qualitative increase or decrease in the number of dendrite branches. RNAi clones were classified as giving rise to positive effects if the overall percentage (average of three to five independent RNAi tests) of animals displaying a defective PVD arborization pattern was ≥20%. Based on these criteria, a total of 11 genes that either promote or suppress the formation of PVD dendrites were retrieved from the screens (Table 1). Interestingly, three of these genes, *unc-116* (Patel et al., 1993; Sakamoto et al., 2005), *dnc-1* (Koushika et al., 2004) and *dli-1* (Koushika et al., 2004) encode proteins (kinesin-1 heavy chain, dynactin and dynein light intermediate chain, respectively) that regulate microtubule-based transport (Table 1), and homologs of another

gene on this list, *bicd-1*, probably regulate minus end-directed microtubule-based transport together with several components of the dynein complex (Table 1) (Swan et al., 1999; Hoogenraad et al., 2001; Matanis et al., 2002; Hoogenraad et al., 2003). Given that a role for *bicd-1* in the developing nervous system had not been previously characterized and the intriguing connection between *bicd-1* and microtubule-based transport machinery, we focused our subsequent analyses on the role of *bicd-1* in PVD dendrite arbor development.

bicd-1(ok2731) mutants phenocopy the *bicd-1* RNAi-induced enhancement of PVD dendrite branching

Posterior to the PVD cell body (tail region), *bicd-1* RNAi led to an increase in the number of ectopic tertiary dendrites along the length of the secondary dendrite (Fig. 3B-D). Quantification revealed that the number of ectopic tertiary dendrites per secondary dendrite was 0.18 in animals fed the empty vector L4440 and 0.9 in *bicd-1* RNAi-treated animals (Fig. 3F). To confirm a requirement for *bicd-1* in PVD dendrite branching, we analyzed a *bicd-1* genetic mutant, *ok2731*. *bicd-1(ok2731)* mutants harbor a 547 bp deletion that eliminates exon 5 and results in the splicing of exon 4 to a cryptic splice site in the middle of exon 6, probably generating a truncated protein that retains partial function (Fig. 3A) (Fridolfsson et al., 2010). Notably, *bicd-1(ok2731)* mutant animals exhibited the same

Fig. 3. *bicd-1(ok2731)* animals phenocopy the *bicd-1* RNAi enhanced-branching defect. (**A**) Genetic position of *bicd-1* on chromosome IV and its exon-intron structure, with the positions of the *ok2731* and *tm3421* mutations indicated. (**B,C**) Schematics of individual PVD dendrite trees present in wild-type (B) and *bicd-1(ok2731)* or *bicd-1* RNAi-treated (C) animals. (**D,E**) *otIs138* animals fed *bicd-1* dsRNA exhibit an enhanced-branching phenotype posterior to the PVD cell body (D). *bicd-1(ok2731)* animals phenocopy the *bicd-1* RNAi enhanced-branching phenotype (E). Purple arrowheads indicate ectopic tertiary dendrites. Asterisks indicate the spermatheca. Anteroposterior orientation is indicated by the white double-headed arrow. (**F**) Quantification of the enhanced-branching phenotype exhibited by *otIs138* young adult animals subjected to *bicd-1* RNAi. (**G**) The PVD enhanced-branching phenotype is first apparent at the young adult stage. n, number of secondary dendrites scored in F and G. Error bars represent s.e.m. ***$P<0.001$ determined by unpaired Student's *t*-test with Bonferroni adjustment. n.s., not significant. Scale bars: 10 μm.

degree of enhanced branching as wild-type animals fed *bicd-1* dsRNA (Fig. 3E,G) and first displayed the phenotype at the young adult stage (Fig. 3G). We also attempted to analyze the *bicd-1(tm3421)* allele, considered to be a genetic null (Fig. 3A) (Fridolfsson et al., 2010). However, owing to the high level of embryonic lethality associated with this allele (Fridolfsson et al., 2010), we were unable to recover young adult *bicd-1(tm3421)* homozygous animals. Cosmid rescue experiments were carried out to confirm that a mutation in the *bicd-1* gene was responsible for the neuronal phenotype exhibited by *bicd-1(ok2731)* animals. Rescue was observed in five out of seven transgenic lines (see Fig. S1 in the supplementary material). These findings, coupled with our observation that wild-type animals subjected to *bicd-1* RNAi exhibited the identical enhanced-branching phenotype displayed by *bicd-1(ok2731)* mutant animals, provide strong evidence that *bicd-1* function is required for the development of the elaborate branching pattern of PVD neurons.

bicd-1(ok2731) genetic mutants exhibit a reduced-branching phenotype distal to the PVD cell body

In *Drosophila*, mutations in components of the minus-end-directed dynein motor complex, *Dynein light intermediate chain* (*Dlic*) and *short wing* (*sw*), result in a decrease in terminal dendrite branching distal to the type IV dendritic arborization (da) neuron ddaC cell body (Satoh et al., 2008; Zheng et al., 2008). Given the previously defined links between Bicaudal D and Dynein in *Drosophila* oogenesis (Swan et al., 1999) and mammalian cell culture systems (Hoogenraad et al., 2001; Hoogenraad et al., 2003; Matanis et al., 2002), we predicted that PVD arbors of *bicd-1(ok2731)* mutants would exhibit a reduction in the number of terminal branches distal to the PVD cell body. To test this hypothesis, the number of terminal branches (quaternary dendrites) was counted in both the distal and proximal regions of the PVD arbor (Fig. 4A). Individual dendritic trees possessing less than two quaternary dendrites
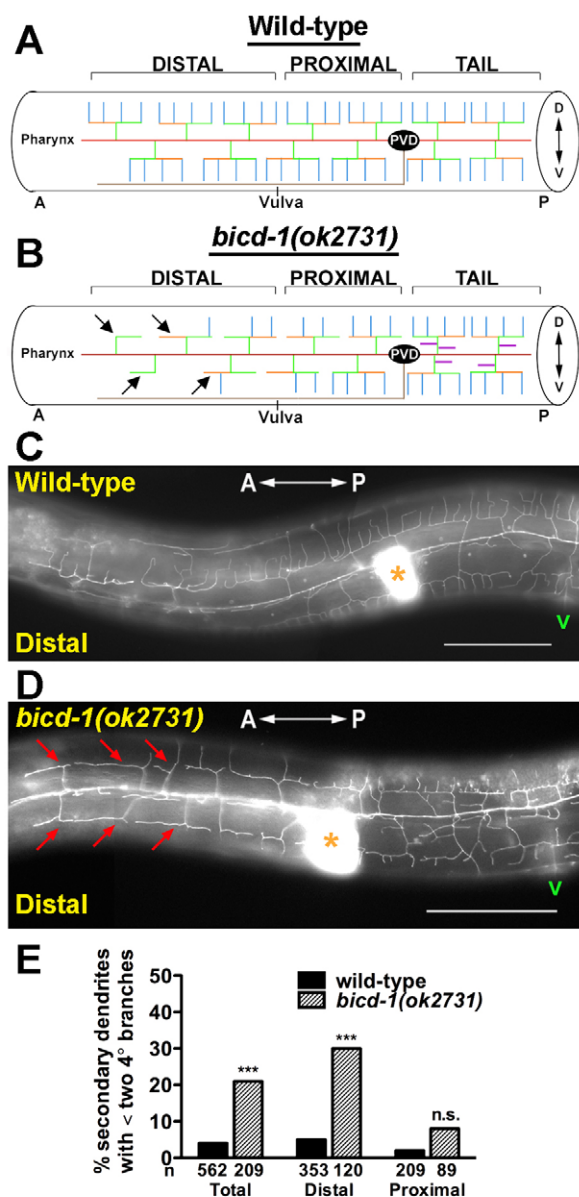
Fig. 4. *bicd-1(ok2731)* animals exhibit a reduction in the number of dendritic branches distal to the PVD cell body. (**A,B**) Schematics of the wild-type (A) and *bicd-1(ok2731)* (B) PVD arborization pattern. 'Distal' specifies the region of the PVD arbor anterior to the vulva and 'proximal' denotes the region between the vulva and the PVD cell body. Arrows indicate individual dendritic trees that possess less than two quaternary dendrites. Dorsoventral orientation is indicated by the double-headed arrow. (**C,D**) Images of the distal regions of wild-type (C) and *bicd-1(ok2731)* (D) PVD arbors of young adult animals (52-58 hours post hatch, room temperature). Asterisks mark the spermatheca and 'v' indicates the position of the vulva. Red arrows point to individual dendritic trees that possess less than two quaternary dendrites. (**E**) Quantification of the branch-reducing phenotype in both the distal and proximal regions of the PVD arbor. n, number of secondary dendrites scored. Error bars represent s.e.m. ***$P<0.001$ determined by chi-square test with Bonferroni adjustment. n.s., not significant. Scale bars: 50 μm.

Fig. 5. *bicd-1::*YFP expression pattern. (**A**) A *bicd-1* transcriptional reporter construct was generated by fusing 6kb of genomic sequence directly upstream of the *bicd-1* ATG to the *yfp/unc-54* 3′UTR cassette. (**B**) Yellow arrows mark YFP protein expression detected in the PVD neuronal cell body and its dendrites at the young adult stage. (**C**) Red arrowheads point to labeled quaternary dendrites of FLP neurons in the head. (**D**) Ventral view of a *bicd-1::*YFP labeled animal. The red and yellow open arrows point to labeled vulva and body wall muscles, respectively. Red arrowheads identify YFP protein expression in the bilaterally symmetrical excretory canals and the yellow arrowhead points to YFP protein expression in the posteriorly directed processes of AVF neurons. Anteroposterior orientation is indicated by the white double-headed arrow. Scale bars: 25 μm in B and C; 50 μm in D.

were considered to exhibit a reduction in branch complexity (Fig. 4B). In wild-type animals, 5% of secondary dendrites analyzed in the distal portion of the PVD dendritic arbor
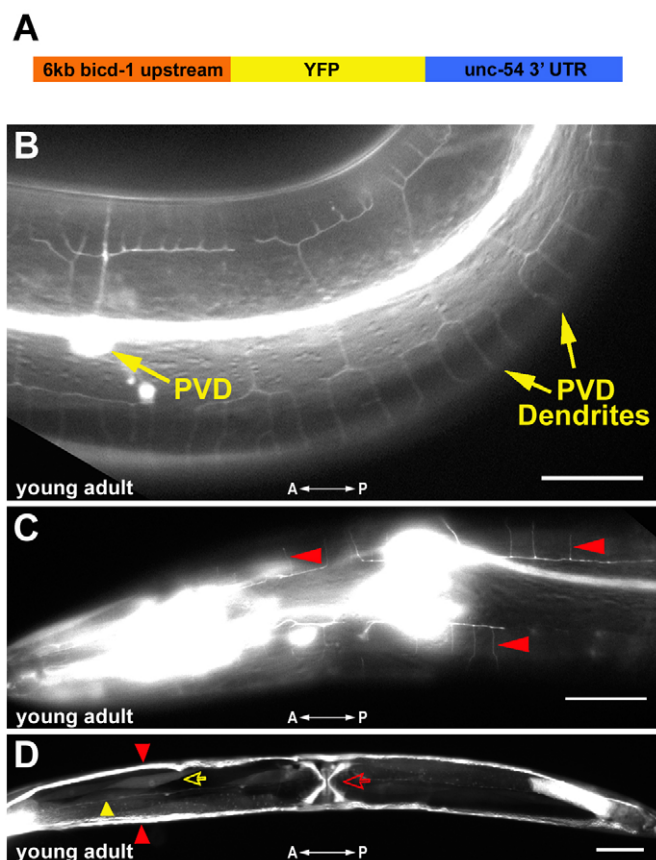
exhibited a reduction in branch complexity (Fig. 4C,E). By contrast, 30% of secondary dendrites analyzed in the distal region of *bicd-1(ok2731)* PVD arbors displayed a reduction in branch complexity (Fig. 4D,E). Notably, this phenotype appeared to be restricted to the distal portion of the arbor as *bicd-1(ok2731)* mutant animals did not exhibit a statistically significant reduction in branch complexity proximal to the PVD cell body compared with wild-type animals (Fig. 4E).

bicd-1 acts in PVD neurons

To gain insights into the expression pattern of *bicd-1* and its possible site(s) of action, we generated a *bicd-1* transcriptional reporter consisting of a 6 kb fragment directly upstream of the *bicd-1* ATG start codon fused to the *yfp/unc-54* 3′UTR cassette (Fig. 5A). Robust *bicd-1::*YFP expression was observed in PVD neurons at the young adult stage, with the onset of expression in PVD first detectable at L4 (Fig. 5B; data not shown). *bicd-1::*YFP expression was also

present in the H-shaped excretory cell, body wall muscle cells, vulva muscle cells and the AVF neuron (Fig. 5D). Notably, FLP neurons, which reside in the head and elaborate PVD-like dendritic arbors, also displayed *bicd-1*::YFP expression (Fig. 5C) and FLP dendrite arbors were malformed in *bicd-1(ok2731)* mutants (see Fig. S2 in the supplementary material). To determine the anatomical focus of action of *bicd-1*, we conducted cell type-specific rescue experiments and genetic mosaic analyses. In the cell type-specific rescue experiments, we investigated whether expression of *bicd-1* cDNA under the control of either a PVD- or a muscle-specific promoter was capable of rescuing the mutant phenotype (Fig. 6A). Selective expression of BICD-1 in PVD neurons partially rescued the enhanced-branching phenotype in three out of four independent transgenic lines, whereas exclusively expressing BICD-1 in muscle cells only weakly rescued the enhanced-branching phenotype in one out of three independent transgenic lines (Fig. 6A and see Fig. S3 in the supplementary material). Furthermore, genetic mosaic analyses revealed that animals that retained wild-type *bicd-1* in the AB.p lineage (which gives rise to the PVD neurons) but not the P1 lineage (which gives rise to 94 out of 95 body wall muscles) exhibited partial rescue of the enhanced-branching *bicd-1(ok2731)* mutant phenotype (Fig. 6B,C). Collectively, these studies support the view that *bicd-1* acts primarily within PVD neurons to regulate the patterning of its dendritic arbors, but might also function in other cells (e.g. muscle).

bicd-1 acts cooperatively with *dhc-1* and *unc-116*

Our large-scale RNAi screen of chromosome IV identified two components of the *C. elegans* dynein motor complex, *dynein light intermediate chain* (*dli-1*) and *dynactin* (*dnc-1*), as probable regulators of PVD dendritic arbors (Table 1). Quantification of the enhanced-branching phenotype displayed by wild-type animals subjected to *dli-1* or *dnc-1* RNAi revealed that the number of ectopic tertiary dendrites per secondary dendrite was 1.05 (*n*=102) and 0.71 (*n*=86), respectively. Animals harboring a genetic mutation in another dynein complex component, *dynein heavy chain* (*dhc-1*), exhibited an enhanced-branching phenotype posterior to the PVD cell body and a reduced-branching phenotype distal to the PVD cell body (Fig. 7A-D and Fig. 8C). The similarities among the *bicd-1*, *dli-1* and *dnc-1* RNAi phenotypes and between the *bicd-1* and *dhc-1* genetic mutant phenotypes, raised the possibility that *bicd-1* genetically interacts with components of the dynein complex to regulate the formation of PVD dendritic arbors. To test this hypothesis, we constructed and analyzed double mutants deficient in both *bicd-1* and *dhc-1*. Posterior to the PVD cell body, *dhc-1(or195);bicd-1(ok2731)* double mutant animals exhibited a statistically significant increase in the number of ectopic tertiary dendrites per secondary dendrite (0.85) compared with the *bicd-1(ok2731)* single mutant (Fig. 8A-C). Because both the *bicd-1(ok2731)* and *dhc-1(or195)* alleles are hypomorphic alleles, these data indicate that *bicd-1* and *dhc-1* probably act cooperatively (either in the same pathway or in parallel pathways) to regulate PVD dendrite branching.

Our candidate-based RNAi screen also identified *unc-116*, a component of the kinesin-1 plus-end-directed motor complex, as a regulator of PVD dendrite branching (Table 1). Consistent with the branching defects observed in *unc-116* RNAi-treated animals, the *unc-116(e2310)* loss-of-function allele exhibited a reduced-branching phenotype in the distal region of the PVD dendritic arbor (Fig. 7E,F). A reduced-branching phenotype, however, was not observed proximal to the PVD cell body (Fig. 7F). Because *unc-116(e2310)* and *bicd-1(ok2731)* mutants each displayed a reduced-branching phenotype in the distal region of the PVD dendritic arbor, we
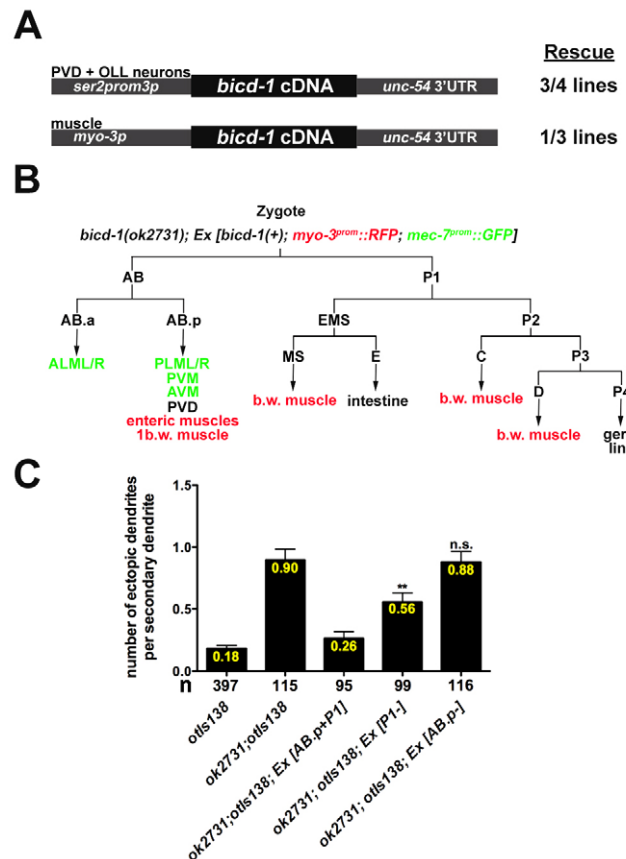

Fig. 6. *bicd-1* acts in PVD neurons. (**A**) *bicd-1* cDNA, expressed under the control of either the PVD specific promoter *ser2prom3* or the muscle-specific promoter *myo-3*, partially rescues the enhanced-branched phenotype. (**B**) Mosaic analysis was conducted using a C43G2 cosmid rescuing line that exhibited complete rescue of the enhanced-branching phenotype (*rzEx111*, see Fig. S1 in the supplementary material). *mec-7::gfp* and *myo-3::rfp* were used to mark the AB.p and P1 lineages, respectively. b.w. muscle, body wall muscle. (**C**) Quantification of the enhanced-branching phenotype present in mosaic animals demonstrates that *bicd-1* acts in PVD neurons. [AB.p+P1] denotes animals that have retained the array in both the AB and P1 lineages. [AB.p-] and [P1-] denote animals that have retained the array in either the P1 or AB.p lineage, respectively. Adult animals scored in the mosaic analyses were initially selected at the L4 stage and scored for rescue 24 hours later. n, number of secondary dendrites scored. Error bars represent s.e.m. **P<0.01 determined by one-way ANOVA with Dunnett's post test.

constructed *unc-116(e2310);bicd-1(ok2731)* double mutants to determine whether *unc-116* and *bicd-1* act cooperatively to regulate the PVD arborization pattern. Although the reduced-branching phenotype in the distal region of the PVD arbor was not significantly enhanced in *unc-116(e2310);bicd-1(ok2731)* double mutants compared with the single mutants, we found that *unc-116(e2310);bicd-1(ok2731)* double mutants exhibited a statistically significant increase in the number of ectopic tertiary dendrites, posterior to the PVD cell body, compared with the *bicd-1(ok2731)* single mutant (Fig. 8D). Because both *bicd-1(ok2731)* and *unc-116(e2310)* are partial loss-of-function alleles, these data indicate that *bicd-1* and *unc-116* probably act cooperatively to regulate PVD dendrite branching, posterior to PVD cell bodies. Together, these
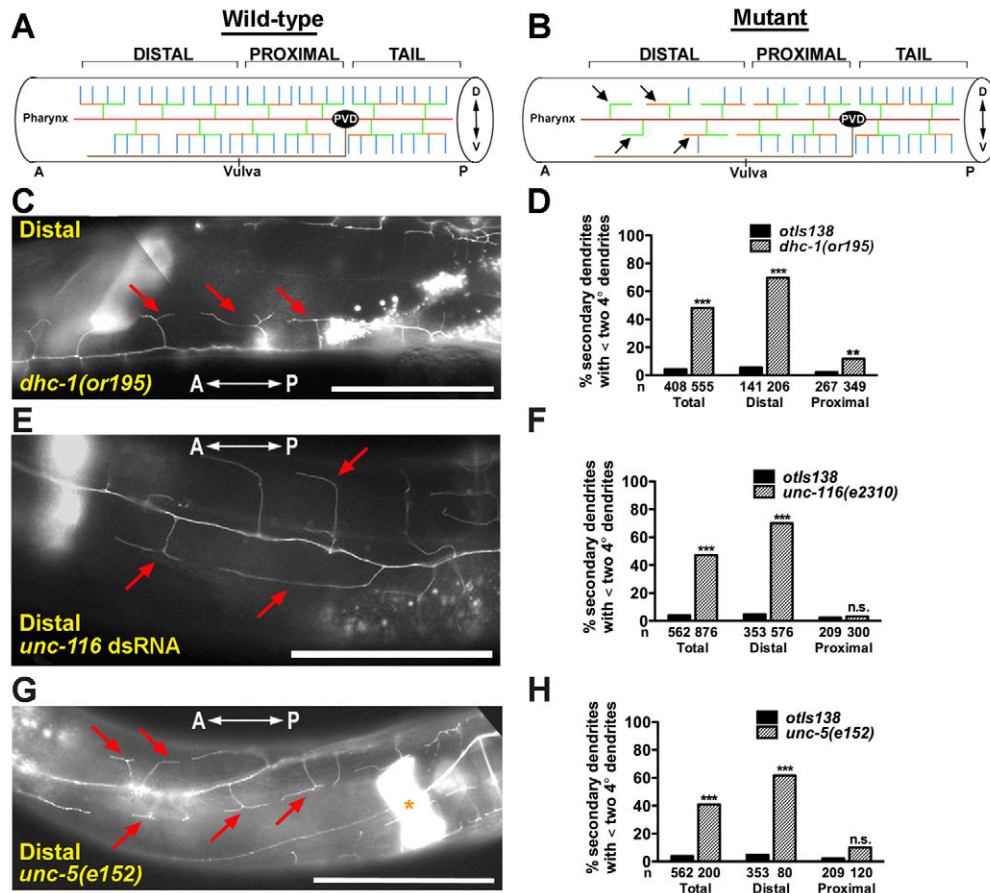
Fig. 7. *dhc-1(or195)*, *unc-116(e2310)* and *unc-5(e152)* mutants possess fewer dendrite branches distal to the PVD cell body.
(**A,B**) Schematics of the wild-type (A) and mutant (B) PVD arborization pattern. 'Distal' specifies the region of the PVD arbor anterior to the vulva and 'proximal' denotes the region between the vulva and the PVD cell body. Arrows point to individual dendritic trees that possess less than two quaternary dendrites. (**C,E,G**) Micrographs of the distal regions of *dhc-1(or195)* (C), *unc-116* RNAi (E) and *unc-5(e152)* (G) PVD arbors. Red arrows point to the absence of quaternary dendrites. The asterisk in G indicates the spermatheca. Anteroposterior orientation is indicated by the white double-headed arrow. (**D,F,H**) Quantification of the branch-reducing phenotype in the distal and proximal regions of the PVD arbor at 25°C (D) and 20°C (F,H). n, number of secondary dendrites scored. *dhc-1(or195)* mutants are temperature sensitive and all analyses utilizing this allele were performed at 25°C. Scale bars: 50 µm. Error bars represent s.e.m. **$P<0.01$, ***$P<0.001$ determined by chi-square test with Bonferroni adjustment. n.s., not significant.

double-mutant analyses indicate that *bicd-1* acts cooperatively with genes encoding components of both minus- and plus-end microtubule-based motors to regulate distinct aspects of PVD dendrite development.

bicd-1 genetically interacts with the repulsive guidance receptor *unc-5*

Our candidate-based RNAi screen identified the repulsive guidance receptor *unc-5* as a probable regulator of PVD dendrite branching, although our initial quantification of the defect revealed a relatively mild phenotype that placed *unc-5* below our arbitrarily defined cut-off for positive clones. Consistent with the *unc-5* RNAi phenotype, the *unc-5(e152)* loss-of-function allele displayed a reduced-branching phenotype in the distal region of the PVD arbor with 62% of the secondary dendrites analyzed elaborating less than two quaternary dendrites compared with 5% in wild-type animals (Fig. 7G,H). By contrast, a reduced-branching phenotype was not observed proximal to the PVD cell body (Fig. 7H). Notably, in the distal region, we observed that neither ventrally directed nor

dorsally directed quaternary dendrites were present (Fig. 7G). Therefore, there was no bias (dorsal versus ventral) to the reduced-branching phenotype. Given the similarity between the *bicd-1* and *unc-5* mutant phenotypes, we constructed *unc-5 bicd-1* double mutants harboring the *unc-5(e53)* null allele and the *bicd-1(ok2731)* allele. We found that *unc-5(e53) bicd-1(ok2731)* double mutants exhibited a robust increase in the number of ectopic tertiary dendrites (1.27) compared with the *bicd-1(ok2731)* single mutant (Fig. 8A,B,E). Next, we generated *unc-5 bicd-1* double mutants using the *unc-5(e152)* allele. This allele is predicted to result in an UNC-5 C-terminal truncation that completely eliminates both the Z-D region and the 'death domain', which are responsible for mediating the UNC-40-independent functions of UNC-5 (Killeen et al., 2002). Notably, the ectopic-branching phenotype of the *unc-5(e152);bicd-1(ok2731)* double mutants (1.48) was at least as severe as that observed in *unc-5(e53);bicd-1(ok2731)* double mutants (1.27) (Fig. 8E). This finding suggests that, in the context of PVD branching, the *unc-5(e152)* allele behaves as a complete loss-of-function allele. Moreover, it
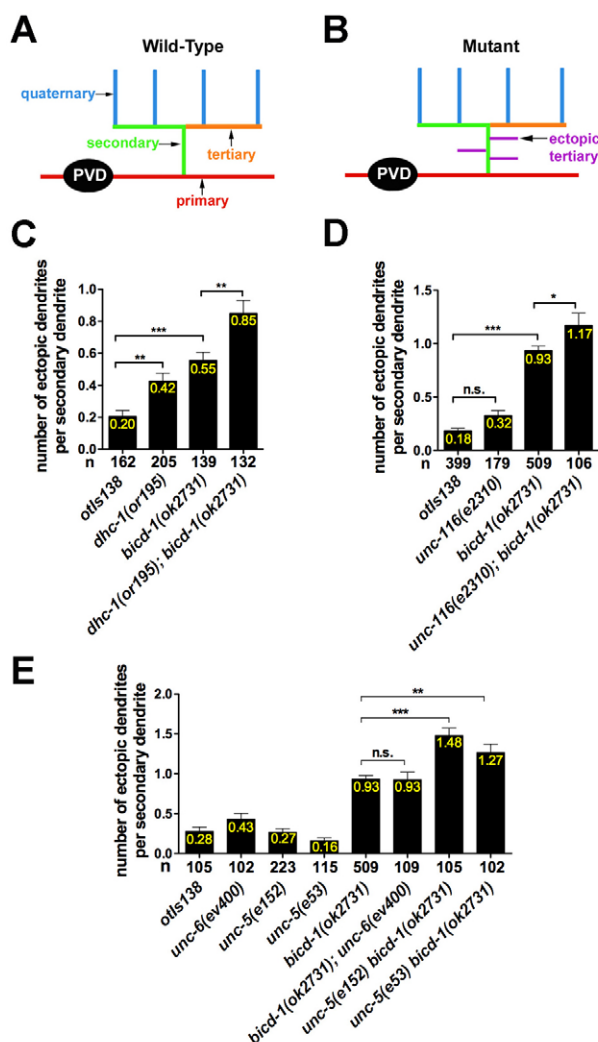
Fig. 8. *bicd-1* genetically interacts with *dhc-1*, *unc-116* and *unc-5* to regulate PVD dendrite branching. (**A**,**B**) Schematic depictions of individual PVD arbors present in wild-type (A) and mutant (B) animals. (**C-E**) Quantification of the enhanced-branching phenotype posterior to the PVD cell body (tail region) at 25°C (C) and 20°C (D,E). n, number of secondary dendrites scored. Error bars represent s.e.m. *$P<0.05$, **$P<0.01$, ***$P<0.001$ determined by one-way ANOVA with Dunnett's post test. n.s., not significant.

indicates that the C-terminal domain of UNC-5 may be crucial for the functional interaction between *unc-5* and *bicd-1*. Although these double mutant data suggest that *bicd-1* and *unc-5* act in parallel pathways to regulate PVD branching, these data do not preclude the possibility that *unc-5* and *bicd-1* also act in the same pathway. Specifically, BICD-1 might aid in the transport of the UNC-5 guidance receptor (acting in the same pathway) along with a variety of additional cargoes (acting in a parallel pathway). We also asked whether *unc-6*, which encodes the netrin ligand for *unc-5*, interacts genetically with *bicd-1*. Unlike *unc-5;bicd-1* double mutant animals, a complete loss of *unc-6* did not enhance the *bicd-1(ok2731)* branching phenotype posterior to the PVD cell body (Fig. 8E). Collectively, these data suggest that *unc-5* has a cryptic role in PVD dendrite development, which appears *unc-6* independent.

DISCUSSION
In this study, we utilize *C. elegans* PVD neurons as a model system for studying dendritic branching. From candidate-based and unbiased RNAi screens we retrieved 11 genes that either promote or suppress the formation of PVD dendrites. We show, for the first time, that *bicd-1* is involved in the development of dendritic branches; an impairment of *bicd-1* function results in a distal-to-proximal shift of PVD dendrite branches. Furthermore, we find that knockdown of either dynein-dynactin or kinesin-1 microtubule-based motor complex components, produces similar PVD dendrite branching phenotypes and that *bicd-1* acts cooperatively with *dhc-1* and *unc-116* to regulate the elaboration of PVD dendritic arbors. Lastly, we demonstrate a novel function for *unc-5* in regulating PVD dendrite branching that appears to be independent of the ligand *unc-6* and requires the cytoplasmic tail of UNC-5.

bicd-1: a novel regulator of dendrite branching
Bicaudal D was initially identified in *Drosophila* as a crucial regulator of anterior-posterior polarity during embryogenesis (Mohler and Wieschaus, 1986; Wharton and Struhl, 1989). More recent studies of *Drosophila* BicD and mammalian BICD1 and BICD2 have provided evidence that Bicaudal D homologs are coiled-coil proteins that function as accessory factors within the dynein-dynactin minus-end-directed motor complex (Hoogenraad et al., 2001; Hoogenraad et al., 2003; Matanis et al., 2002; Swan et al., 1999). In non-neuronal cells, Bicaudal D has been implicated as a key modulator of mRNA, organelle and lipid droplet transport as well as microtubule anchoring at the centrosome (Bullock and Ish-Horowicz, 2001; Fridolfsson et al., 2010; Fumoto et al., 2006; Larsen et al., 2008; Swan et al., 1999). In neurons, it has been found to play a role in retrograde transport in neurites of SK-N-SH cells (Wanschers et al., 2007), nuclear migration in *Drosophila* photoreceptor cells (Swan et al., 1999) and synaptic vesicle recycling at the *Drosophila* neuromuscular junction (Li et al., 2010). In this study, we identify a novel role for the *C. elegans* homolog of *Bicaudal D*, *bicd-1*, in neuronal dendrite branching. Specifically, we show that both *bicd-1* RNAi-treated animals and *bicd-1* deletion mutants exhibit an enhanced PVD dendrite branching phenotype posterior and proximal to the PVD cell body, and a reduced-branching phenotype distal to PVD. Furthermore, both cell type-specific rescue experiments and genetic mosaic analyses suggest that *bicd-1* acts primarily in PVD neurons.

A proposed mechanism for BICD-1 function
It has recently been shown that the minus-end-directed dynein motor complex has a key role in establishing the dendritic arborization pattern of class IV da neurons in *Drosophila* (Satoh et al., 2008; Zheng et al., 2008). Specifically, mutations in the dynein complex components *Dlic*, *sw* and *Dhc1*, as well as a disruption in the function of the dynein-associated factors *Lissencephaly-1* (*Lis-1*) and *lava lamp* (*lva*), result in a decrease in the number of terminal branches in the distal arbor and an increase in the number of ectopic branches in more proximal regions of the arbor (Satoh et al., 2008; Ye et al., 2007; Zheng et al., 2008). Notably, the distribution of Golgi outposts (satellite Golgi cisternae that are required for dendritic growth and branching) exhibited a corresponding shift from a distal to a proximal position within *dlic* and Lva mutant dendritic arbors (Horton and Ehlers, 2003; Horton et al., 2005; Ye et al., 2007; Zheng et al., 2008). Thus, the dynein motor complex might normally act to transport Golgi outposts within the dendritic arbor in order to facilitate the growth of dendritic branches (Zheng et al., 2008). Consistent with these

observations, we find that the perturbation of dynein-associated *bicd-1* or core components of the dynein motor complex results in an analogous distal-to-proximal shift in the distribution of PVD dendrite branches. Assuming that Golgi outposts are also present in *C. elegans* PVD dendrites, these phenotypic similarities raise the possibility that *bicd-1*, in conjunction with the dynein motor complex, is involved in the transport and localization of these specialized Golgi formations within PVD dendritic arbors. Like *Drosophila* Lva, mammalian BICD1 and BICD2 are coiled-coil golgin adaptors that also bind to dynein and dynactin and are localized to the Golgi network (Hoogenraad et al., 2001; Matanis et al., 2002). Furthermore, knockdown of mammalian BICD1 and BICD2 results in disruption of Golgi morphology (Fumoto et al., 2006). Given that there are no known *C. elegans* homologs of *lva*, it is tempting to speculate that *C. elegans* BICD-1 could function in a similar manner to *Drosophila* Lva to not only transport Golgi outposts but also preserve their morphology.

We also report that animals harboring a mutation in the kinesin heavy chain ortholog *unc-116*, just like *bicd-1* and *dhc-1* mutant animals, exhibit a reduced-branching phenotype distal to the PVD cell body. In addition, we show that the *unc-116(e2310)* mutation enhances the *bicd-1(ok2731)* enhanced-branching phenotype that is present posterior to the PVD cell body, leading us to conclude that *unc-116* and *bicd-1* act cooperatively to regulate the PVD dendrite branching pattern. In *Drosophila* class IV da neurons, it has been reported that animals mutant for *Kinesin heavy chain* (*Khc*) also exhibit dendritic branching defects identical to those observed in animals mutant for dynein complex components, raising the possibility that the kinesin motor might be responsible for transporting the dynein complex back to the cell body once dynein has unloaded its cargo (Satoh et al., 2008). Alternatively, we envisage a scenario in which the dynein and kinesin motors participate in bidirectional transport. Specifically, a single cargo would undergo net polarized transport along a single microtubule through the actions of the opposing motors (Welte, 2004). This bidirectional transport could allow for the navigation of cargo around obstacles (organelles, vesicles, etc.), thereby improving the efficiency of net transport (Welte, 2004). Recent evidence suggests that nuclear migration across *C. elegans* hyp7 embryonic hypodermal precursor cells is facilitated by the coordinated action of both dynein and kinesin-1 motors, with kinesin-1 acting to move nuclei forward and dynein acting to navigate obstacles by backward movements (Fridolfsson and Starr, 2010). Assuming that microtubules are oriented with their minus-ends distal in PVD neurons, as they are in *Drosophila* class IV neuronal dendritic arbors (Satoh et al., 2008; Zheng et al., 2008), we speculate that dynein motors direct the forward transport of cargo into PVD dendrites (towards microtubule minus-ends), whereas kinesin-1 motors facilitate the navigation of cargo around the intracellular milieu via transport in the reverse direction (towards microtubule plus-ends). Specifically, in *unc-116(e2310)* mutants, the impaired kinesin-1 complex would be incapable of navigating cargo around obstacles in its path, thereby inhibiting the dynein complex from transporting cargo towards the periphery of the PVD dendritic arbor. This disruption of *unc-116* function would lead to a PVD reduced-branching phenotype similar to that observed in *bicd-1* and dynein mutants. In *unc-116(e2310);bicd-1(ok2731)* double mutant animals, both the ability to transport cargo in the anterograde direction and to navigate around obstacles would be perturbed, leading to an enhancement of the branching phenotype present in *bicd-1(ok2731)* animals posterior to the PVD cell body.

A novel role for *unc-5* in regulating dendrite morphogenesis

C. elegans UNC-5 is a conserved repulsive guidance receptor that functions cell autonomously to mediate the dorsalward migration of cells and pioneer axons in an UNC-6-dependent fashion (Hamelin et al., 1993; Hedgecock et al., 1990; Leung-Hagesteijn et al., 1992; Su et al., 2000). We find that animals subjected to *unc-5* RNAi or harboring the *unc-5(e152)* genetic mutation exhibit a reduced-branching phenotype distal to the PVD cell body. Although UNC-5 has not been previously implicated as a regulator of dendritic branching in any model system, it is interesting to note that vertebrate *Unc5b* can function as either an anti- (Lu et al., 2004) or pro-angiogenic (Navankasattusas et al., 2008) factor to regulate the branching of vasculature during embryonic development. In addition, *Unc5b* is localized to the tip and neck region of embryonic mouse distal lung endoderm during a period when lung epithelial tubes exhibit extensive branching (Dalvin et al., 2003; Liu et al., 2004).

Although the detailed mechanisms underlying the transport and subcellular localization of UNC-5 remain to be defined, it was recently reported that UNC-5::GFP is associated with small vesicles in DD and VD motor neuron axons and cell bodies (Ogura and Goshima, 2006). Together with our findings, this raises the possibility that the dynein motor complex within the PVD dendritic arbor transports UNC-5-containing vesicles. Notably, the *unc-5(e152)* allele harbors a non-sense mutation (Q507STOP) that results in truncation of the UNC-5 cytoplasmic domain at the beginning of the ZU-5 motif (Killeen et al., 2002). In addition, multiple dynein motors are required to transport a single cargo in vivo, and the recruitment of multiple dyneins to a single cargo is required for facilitating long distance transport in vitro (Mallik et al., 2005). Accordingly, the cytoplasmic domain of UNC-5 may be necessary for the recruitment of multiple dynein motors that would facilitate its long distance transport to the distal region of the PVD dendritic arbor. The cytoplasmic truncation associated with *unc-5(e152)* mutants might disrupt the recruitment of multiple motors, thereby limiting the distance that UNC-5 can be transported along PVD dendrites. Furthermore, PVD neurons extend primary dendritic process that run almost the entire length of the animal, with the anterior primary dendrite extending a significantly longer distance away from the PVD cell body than the posterior primary dendrite. A lack of UNC-5 at the distal-most segment of the anterior primary process (anterior to the vulva) may account for the significantly reduced (or lack of) dendritic branching in the distal region of the PVD arbor, as observed in *unc-5(e152)* mutants. Our double mutant analyses, using both the *unc-5* loss-of-function allele *e152* as well as the *unc-5* molecular null allele *e53*, suggest that *unc-5* and *bicd-1* act cooperatively to regulate the branching pattern of PVD dendrites. Surprisingly, we find that a complete loss of *unc-6*, the netrin ligand for *unc-5*, did not enhance the *bicd-1* PVD branching phenotype, suggesting that *unc-5* might act independently of *unc-6*.

References
Ashrafi, K., Chang, F. Y., Watts, J. L., Fraser, A. G., Kamath, R. S., Ahringer, J. and Ruvkun, G. (2003). Genome-wide RNAi analysis of Caenorhabditis elegans fat regulatory genes. *Nature* **421**, 268-272.

Baens, M. and Marynen, P. (1997). A human homologue (BICD1) of the Drosophila bicaudal-D gene. *Genomics* **45**, 601-606.

Brenner, S. (1974). The genetics of Caenorhabditis elegans. *Genetics* **77**, 71-94.

Bullock, S. L. and Ish-Horowicz, D. (2001). Conserved signals and machinery for RNA transport in Drosophila oogenesis and embryogenesis. *Nature* **414**, 611-616.

Bullock, S. L., Nicol, A., Gross, S. P. and Zicha, D. (2006). Guidance of bidirectional motor complexes by mRNA cargoes through control of dynein number and activity. *Curr. Biol.* **16**, 1447-1452.

Bülow, H. E., Berry, K. L., Topper, L. H., Peles, E. and Hobert, O. (2002). Heparan sulfate proteoglycan-dependent induction of axon branching and axon misrouting by the Kallmann syndrome gene kal-1. *Proc. Natl. Acad. Sci. USA* **99**, 6346-6351.

Chatzigeorgiou, M., Yoo, S., Watson, J. D., Lee, W. H., Spencer, W. C., Kindt, K. S., Hwang, S. W., Miller, D. M., III, Treinin, M., Driscoll, M. et al. (2010). Specific roles for DEG/ENaC and TRP channels in touch and thermosensation in C. elegans nociceptors. *Nat. Neurosci.* **13**, 861-868.

Corty, M. M., Matthews, B. J. and Grueber, W. B. (2009). Molecules and mechanisms of dendrite development in Drosophila. *Development* **136**, 1049-1061.

Dalvin, S., Anselmo, M. A., Prodhan, P., Komatsuzaki, K., Schnitzer, J. J. and Kinane, T. B. (2003). Expression of Netrin-1 and its two receptors DCC and UNC5H2 in the developing mouse lung. *Gene. Expr. Patterns* **3**, 279-283.

Fire, A., Xu, S., Montgomery, M. K., Kostas, S. A., Driver, S. E. and Mello, C. C. (1998). Potent and specific genetic interference by double-stranded RNA in Caenorhabditis elegans. *Nature* **391**, 806-811.

Fraser, A. G., Kamath, R. S., Zipperlen, P., Martinez-Campos, M., Sohrmann, M. and Ahringer, J. (2000). Functional genomic analysis of C. elegans chromosome I by systematic RNA interference. *Nature* **408**, 325-330.

Fridolfsson, H. N. and Starr, D. A. (2010). Kinesin-1 and dynein at the nuclear envelope mediate the bidirectional migrations of nuclei. *J. Cell Biol.* **191**, 115-128.

Fridolfsson, H. N., Ly, N., Meyerzon, M. and Starr, D. A. (2010). UNC-83 coordinates kinesin-1 and dynein activities at the nuclear envelope during nuclear migration. *Dev. Biol.* **338**, 237-250.

Fumoto, K., Hoogenraad, C. C. and Kikuchi, A. (2006). GSK-3beta-regulated interaction of BICD with dynein is involved in microtubule anchorage at centrosome. *EMBO. J.* **25**, 5670-5682.

Grueber, W. B., Yang, C. H., Ye, B. and Jan, Y. N. (2005). The development of neuronal morphology in insects. *Curr. Biol.* **15**, R730-R738.

Hamelin, M., Zhou, Y., Su, M. W., Scott, I. M. and Culotti, J. G. (1993). Expression of the UNC-5 guidance receptor in the touch neurons of C. elegans steers their axons dorsally. *Nature* **364**, 327-330.

Hamilton, B., Dong, Y., Shindo, M., Liu, W., Odell, I., Ruvkun, G. and Lee, S. S. (2005). A systematic RNAi screen for longevity genes in C. elegans. *Genes Dev.* **19**, 1544-1555.

Hausser, M., Spruston, N. and Stuart, G. J. (2000). Diversity and dynamics of dendritic signaling. *Science* **290**, 739-744.

Hedgecock, E. M., Culotti, J. G. and Hall, D. H. (1990). The unc-5, unc-6, and unc-40 genes guide circumferential migrations of pioneer axons and mesodermal cells on the epidermis in C. elegans. *Neuron* **4**, 61-85.

Hobert, O. (2002). PCR fusion-based approach to create reporter gene constructs for expression analysis in transgenic C. elegans. *Biotechniques* **32**, 728-730.

Hoogenraad, C. C., Akhmanova, A., Howell, S. A., Dortland, B. R., De Zeeuw, C. I., Willemsen, R., Visser, P., Grosveld, F. and Galjart, N. (2001). Mammalian Golgi-associated Bicaudal-D2 functions in the dynein-dynactin pathway by interacting with these complexes. *EMBO J.* **20**, 4041-4054.

Hoogenraad, C. C., Wulf, P., Schiefermeier, N., Stepanova, T., Galjart, N., Small, J. V., Grosveld, F., de Zeeuw, C. I. and Akhmanova, A. (2003). Bicaudal D induces selective dynein-mediated microtubule minus end-directed transport. *EMBO J.* **22**, 6004-6015.

Horton, A. C. and Ehlers, M. D. (2003). Dual modes of endoplasmic reticulum-to-Golgi transport in dendrites revealed by live-cell imaging. *J. Neurosci.* **23**, 6188-6199.

Horton, A. C., Rácz, B., Monson, E. E., Lin, A. L., Weinberg, R. J. and Ehlers, M. D. (2005). Polarized secretory trafficking directs cargo for asymmetric dendrite growth and morphogenesis. *Neuron* **48**, 757-771.

Jan, Y. N. and Jan, L. Y. (2010). Branching out: mechanisms of dendritic arborization. *Nat. Rev. Neurosci.* **11**, 316-328.

Kakimoto, T., Katoh, H. and Negishi, M. (2006). Regulation of neuronal morphology by Toca-1, an F-BAR/EFC protein that induces plasma membrane invagination. *J. Biol. Chem.* **281**, 29042-29053.

Kamath, R. S. and Ahringer, J. (2003). Genome-wide RNAi screening in Caenorhabditis elegans. *Methods* **30**, 313-321.

Kamath, R. S., Fraser, A. G., Dong, Y., Poulin, G., Durbin, R., Gotta, M., Kanapin, A., Le Bot, N., Moreno, S., Sohrmann, M. et al. (2003). Systematic functional analysis of the Caenorhabditis elegans genome using RNAi. *Nature* **421**, 231-237.

Killeen, M., Tong, J., Krizus, A., Steven, R., Scott, I., Pawson, T. and Culotti, J. (2002). UNC-5 function requires phosphorylation of cytoplasmic tyrosine 482, but its UNC-40-independent functions also require a region between the ZU-5 and death domains. *Dev. Biol.* **251**, 348-366.

Kim, K. and Li, C. (2004). Expression and regulation of an FMRFamide-related neuropeptide gene family in Caenorhabditis elegans. *J. Comp. Neurol.* **475**, 540-550.

Kim, M. J., Liu, I. H., Song, Y., Lee, J. A., Halfter, W., Balice-Gordon, R. J., Linney, E. and Cole, G. J. (2007). Agrin is required for posterior development and motor axon outgrowth and branching in embryonic zebrafish. *Glycobiology* **17**, 231-247.

Koushika, S. P., Schaefer, A. M., Vincent, R., Willis, J. H., Bowerman, B. and Nonet, M. L. (2004). Mutations in Caenorhabditis elegans cytoplasmic dynein components reveal specificity of neuronal retrograde cargo. *J. Neurosci.* **24**, 3907-3916.

Larsen, K. S., Xu, J., Cermelli, S., Shu, Z. and Gross, S. P. (2008). BicaudalD actively regulates microtubule motor activity in lipid droplet transport. *PLoS ONE* **3**, e3763.

Leung-Hagesteijn, C., Spence, A. M., Stern, B. D., Zhou, Y., Su, M. W., Hedgecock, E. M. and Culotti, J. G. (1992). UNC-5, a transmembrane protein with immunoglobulin and thrombospondin type 1 domains, guides cell and pioneer axon migrations in C. elegans. *Cell* **71**, 289-299.

Li, X., Kuromi, H., Briggs, L., Green, D. B., Rocha, J. J., Sweeney, S. T. and Bullock, S. L. (2010). Bicaudal-D binds clathrin heavy chain to promote its transport and augments synaptic vesicle recycling. *EMBO J.* **29**, 992-1006.

Liu, Y., Stein, E., Oliver, T., Li, Y., Brunken, W. J., Koch, M., Tessier-Lavigne, M. and Hogan, B. L. M. (2004). Novel role for netrins in regulating epithelial behavior during lung branching morphogenesis. *Curr. Biol.* **14**, 897-905.

Lu, X., le Noble, F., Yuan, L., Jiang, Q., de Lafarge, B., Sugiyama, D., Breant, C., Claes, F., De Smet, F., Thomas, J. L. et al. (2004). The netrin receptor UNC5B mediates guidance events controlling morphogenesis of the vascular system. *Nature* **432**, 179-186.

Mallik, R., Petrov, D., Lex, S. A., King, S. J. and Gross, S. P. (2005). Building complexity: an in vitro study of cytoplasmic dynein with in vivo implications. *Curr. Biol.* **15**, 2075-2085.

Marshak, S., Nikolakopoulou, A. M., Dirks, R., Martens, G. J. and Cohen-Cory, S. (2007). Cell-autonomous TrkB signaling in presynaptic retinal ganglion cells mediates axon arbor growth and synapse maturation during the establishment of retinotectal synaptic connectivity. *J. Neurosci.* **27**, 2444-2456.

Matanis, T., Akhmanova, A., Wulf, P., Del Nery, E., Weide, T., Stepanova, T., Galjart, N., Grosveld, F., Goud, B., De Zeeuw, C. I. et al. (2002). Bicaudal-D regulates COPI-independent Golgi-ER transport by recruiting the dynein-dynactin motor complex. *Nat. Cell Biol.* **4**, 986-992.

Miyashita, T., Yeo, S. Y., Hirate, Y., Segawa, H., Wada, H., Little, M. H., Yamada, T., Takahashi, N. and Okamoto, H. (2004). PlexinA4 is necessary as a downstream target of Islet2 to mediate Slit signaling for promotion of sensory axon branching. *Development* **131**, 3705-3715.

Mohler, J. and Wieschaus, E. F. (1986). Dominant maternal-effect mutations of Drosophila melanogaster causing the production of double-abdomen embryos. *Genetics* **112**, 803-822.

Navankasattusas, S., Whitehead, K. J., Suli, A., Sorensen, L. K., Lim, A. H., Zhao, J., Park, K. W., Wythe, J. D., Thomas, K. R., Chien, C. B. et al. (2008). The netrin receptor UNC5B promotes angiogenesis in specific vascular beds. *Development* **135**, 659-667.

Ogura, K. and Goshima, Y. (2006). The autophagy-related kinase UNC-51 and its binding partner UNC-14 regulate the subcellular localization of the Netrin receptor UNC-5 in Caenorhabditis elegans. *Development* **133**, 3441-3450.

Oren-Suissa, M., Hall, D. H., Treinin, M., Shemer, G. and Podbilewicz, B. (2010). The fusogen EFF-1 controls sculpting of mechanosensory dendrites. *Science* **328**, 1285-1288.

Patel, N., Thierry-Mieg, D. and Mancillas, J. R. (1993). Cloning by insertional mutagenesis of a cDNA encoding Caenorhabditis elegans kinesin heavy chain. *Proc. Natl. Acad. Sci. USA* **90**, 9181-9185.

Sakamoto, R., Byrd, D. T., Brown, H. M., Hisamoto, N., Matsumoto, K. and Jin, Y. (2005). The Caenorhabditis elegans UNC-14 RUN domain protein binds

to the Kinesin-1 and UNC-16 complex and regulates synaptic vesicle localization. *Mol. Biol. Cell* **16**, 483-496.

Satoh, D., Sato, D., Tsuyama, T., Saito, M., Ohkura, H., Rolls, M. M., Ishikawa, F. and Uemura, T. (2008). Spatial control of branching within dendritic arbors by dynein-dependent transport of Rab5-endosomes. *Nat. Cell Biol.* **10**, 1164-1171.

Schmitz, C., Kinge, P. and Hutter, H. (2007). Axon guidance genes identified in a large-scale RNAi screen using the RNAi-hypersensitive Caenorhabditis elegans strain nre-1(hd20) lin-15b(hd126). *Proc. Natl. Acad. Sci. USA* **104**, 834-839.

Smith, C. J., Watson, J. D., Spencer, W. C., O'Brien, T., Cha, B., Albeg, A., Treinin, M. and Miller, D. M, III (2010). Time-lapse imaging and cell-specific expression profiling reveal dynamic branching and molecular determinants of a multi-dendritic nociceptor in C. elegans. *Dev. Biol.* **345**, 18-33.

Struckhoff, E. C. and Lundquist, E. A. (2003). The actin-binding protein UNC-115 is an effector of Rac signaling during axon pathfinding in C. elegans. *Development* **130**, 693-704.

Su, M., Merz, D. C., Killeen, M. T., Zhou, Y., Zheng, H., Kramer, J. M., Hedgecock, E. M. and Culotti, J. G. (2000). Regulation of the UNC-5 netrin receptor initiates the first reorientation of migrating distal tip cells in Caenorhabditis elegans. *Development* **127**, 585-594.

Suter, B., Romberg, L. M. and Steward, R. (1989). Bicaudal-D, a Drosophila gene involved in developmental asymmetry: localized transcript accumulation in ovaries and sequence similarity to myosin heavy chain tail domains. *Genes Dev.* **3**, 1957-1968.

Swan, A., Nguyen, T. and Suter, B. (1999). Drosophila Lissencephaly-1 functions with Bic-D and dynein in oocyte determination and nuclear positioning. *Nat. Cell Biol.* **1**, 444-449.

Tsalik, E. L., Niacaris, T., Wenick, A. S., Pau, K., Avery, L. and Hobert, O. (2003). LIM homeobox gene-dependent expression of biogenic amine receptors in restricted regions of the C. elegans nervous system. *Dev. Biol.* **263**, 81-102.

Urbanska, M., Blazejczyk, M. and Jaworski, J. (2008). Molecular Basis of Dendrite Arborization. *Acta Neurobiol. Exp. (Wars.)* **68**, 264-288.

Wanschers, B. F. J., van de Vorstenbosch, R., Schlager, M. A., Splinter, D., Akhmanova, A., Hoogenraad, C. C., Wieringa, B. and Fransen, J. A. M. (2007). A role for the Rab6B Bicaudal-D1 interaction in retrograde transport in neuronal cells. *Exp. Cell Res.* **313**, 3408-3420.

Way, J. C. and Chalfie, M. (1988). mec-3, a homeobox-containing gene that specifies differentiation of the touch receptor neurons in C. elegans. *Cell* **54**, 5-16.

Way, J. C. and Chalfie, M. (1989). The mec-3 gene of Caenorhabditis elegans requires its own product for maintained expression and is expressed in three neuronal cell types. *Genes Dev.* **3**, 1823-1833.

Welte, M. A. (2004). Bidirectional transport along microtubules. *Curr. Biol.* **14**, R525-R537.

Wharton, R. P. and Struhl, G. (1989). Structure of the Drosophila BicaudalD protein and its role in localizing the posterior determinant nanos. *Cell* **59**, 881-892.

Wolters, N. M. and MacKeigan, J. P. (2008). From sequence to function: using RNAi to elucidate mechanisms of human disease. *Cell Death Differ.* **15**, 809-819.

Yassin, L., Gillo, B., Kahan, T., Halevi, S., Eshel, M., Treinin, M. (2001). Characterization of the DEG-3/DES-2 receptor: a nicotinic acetylcholine receptor that mutates to cause neuronal degeneration. *Mol. Cell. Neurosci.* **17**, 589-599.

Ye, B., Zhang, Y., Song, W., Younger, S. H., Jan, L. Y. and Jan, Y. N. (2007). Growing dendrites and axons differ in their reliance on the secretory pathway. *Cell* **130**, 717-729.

Zheng, Y., Wildonger, J., Ye, B., Zhang, Y., Kita, A., Younger, S. H., Zimmerman, S., Jan, L. Y. and Jan, Y. N. (2008). Dynein is required for polarized dendritic transport and uniform microtubule orientation in axons. *Nat. Cell Biol.* **10**, 1172-1180.

Table S1. 137 RNAi clones tested in the candidate-based RNAi screen

Chromosome	Gene name	GenePair name	Branching defect (%)	Total (n)
X	unc-115	F09B9.2	65	20
IV	mec-3	F01D4.6	39	18
II	unc-52	ZC101.2	31	16
X	lon-2	C39E6.1	25	20
III	F54D8.6	F54D8.6	20	20
I	F47B3.1	F47B3.1	19	21
III	unc-86	C30A5.7	19	27
I	wwp-1	Y65B4BR.4	17	12
III	unc-116	R05D3.7	16	19
I	W03D8.8	W03D8.8	15	20
I	lin-59	T12F5.4	15	20
X	hst-2	C34F6.4	13	23
IV	unc-5	B0273.4	11	18
I	F46F11.9	F46F11.9	10	20
I	lem-3	F42H11.2	10	20
I	Y106G6A.2	Y106G6A.2	10	20
I	ZK973.8	ZK973.8	8	13
V	unc-70	K11C4.3	7	15
III	K04H4.2	K04H4.2	5	19
I	unc-73	F55C7.7	5	20
I	C09D4.1	C09D4.1	5	20
I	T24D1.3	T24D1.3	5	20
I	smd-1	F47G4.7	5	20
I	sur-2	F39B2.4	5	20
I	Y47G6A.29	Y47G6A.29	5	20
III	ceh-13	R13A5.5	5	20
I	mec-6	W02D3.3	5	21
III	dpy-27	R13G10.1	5	21
I	T05E8.3	T05E8.3	0	15
X	hst-6	Y34B4A.3	0	16
III	T07A5.2	T07A5.2	0	19
V	des-2	T26H10.1	0	19
X	efn-3	F15A2.5	0	20
V	unc-76	C01G10.11	0	22
V	egl-46	K11G9.4	0	23
I	C24G7.1	C24G7.1	0	20
I	C41D11.2	C41D11.2	0	9
I	B0041.5	B0041.5	0	16
I	F48C1.4	F48C1.4	0	15
I	unc-40	T19B4.7	0	20
I	hmg-3	C32F10.5	0	20
I	F26B1.1	F26B1.1	0	20
I	ZC328.2	ZC328.2	0	17
I	mdt-18	C55B7.9	0	20
I	ZC581.9	ZC581.9	0	20
I	C17F3.1	C17F3.1	0	20
I	T23B3.4	T23B3.4	0	20
I	lbp-5	W02D3.7	0	20
I	pqn-20	C37A2.2	0	17
I	unc-13	ZK524.2	0	20
I	F29D11.2	F29D11.2	0	19
I	nmy-2	F20G4.3	0	20
I	F43G9.3	F43G9.3	0	15
I	F26E4.5	F26E4.5	0	20
I	nas-5	T23H4.3	0	19
I	Y106G6A.4	Y106G6A.4	0	20
I	Y106G6A.5	Y106G6A.5	0	15
I	F10G8.4	F10G8.4	0	13
I	F25D7.1	F25D7.1	0	20

I	Y106G6H.8	Y106G6H.8	0	20
I	ced-1	Y47H9C.4	0	20
I	T15D6.9	T15D6.9	0	20
I	E03H4.1	E03H4.1	0	21
I	unc-101	K11D2.3	0	20
I	Y18D10A.21	Y18D10A.21	0	20
I	Y37H9A.1	Y37H9A.1	0	19
I	Y63D3A.9	Y63D3A.9	0	20
I	pry-1	C37A5.9	0	12
I	Y95B8A.7	Y95B8A.7	0	20
I	pde-6	Y95B8A.10	0	12
I	unc-95	Y105E8A.6	0	20
I	Y105E8A.23	Y105E8A.23	0	20
I	Y105E8B.9	Y105E8B.9	0	20
I	Y48G1C.8	Y48G1C.8	0	20
I	Y34D9A.3	Y34D9A.3	0	20
I	lpd-3	Y47G6A.23	0	14
I	rnp-6	Y47G6A.20	0	20
I	mig-1	Y34D9B.1	0	25
I	goa-1	C26C6.2	0	20
I	kal-1	K03D10.1	0	20
I	smp-1	Y54E5B.1	0	21
II	hst-3.1	F40H3.5	0	20
II	unc-104	C52E12.2	0	20
II	glr-4	C06A8.9	0	20
II	agr-1	F41G3.12	0	20
II	unc-53	F45E10.1	0	19
II	plx-2	K04B12.1	0	20
III	F59A2.6	F59A2.6	0	19
III	hum-5	T02C12.1	0	21
III	ZC155.7	ZC155.7	0	20
III	cdh-4	F25F2.2	0	17
III	grl-22	W03A5.3	0	20
III	D1044.2	D1044.2	0	25
III	hse-5	B0285.5	0	20
III	T04C9.2	T04C9.2	0	20
III	lin-39	C07H6.7	0	17
III	F44E2.4	F44E2.4	0	20
III	D2007.2	D2007.2	0	18
III	F54H12.2	F54H12.2	0	20
III	C40H1.3	C40H1.3	0	18
III	tbx-9	T07C4.6	0	11
III	Y52D3.1	Y52D3.1	0	20
III	ZK1128.5	ZK1128.5	0	20
III	Y43F4B.3	Y43F4B.3	0	20
III	Y56A3A.21	Y56A3A.21	0	18
III	Y37D8A.7	Y37D8A.7	0	20
III	cua-1	Y76A2A.2	0	20
III	unc-71	Y37D8A.13	0	20
III	T28A8.3	T28A8.3	0	19
III	dhs-9	Y32H12A.3	0	20
III	mdt-21	C24H11.9	0	20
III	pst-2	F54E7.1	0	20
III	unc-32	ZK637.8	0	8
III	eat-4	ZK512.6	0	20
III	ina-1	F54G8.3	0	20
IV	osm-9	B0212.5	0	20
IV	efn-4	F56A11.3	0	20
IV	unc-44	B0350.2	0	22
IV	wsp-1	C07G1.4	0	20
IV	hst-1	F08B4.6	0	20
IV	vab-2	Y37E11AR.6	0	20
IV	plx-1	Y55F3AL.1	0	16

V	mec-9	C50H2.3	0	20
V	deg-3	K03B8.9	0	22
V	sma-1	R31.1	0	20
V	pkc-1	F57F5.5	0	21
X	Toca-1	F09E10.8	0	21
X	sax-3	ZK377.2	0	20
X	nlp-11	C01C4.1	0	7
X	sul-1	K09C4.8	0	20
X	unc-6	F41C6.1	0	20
X	trk-1	D1073.1	0	20
X	him-4	F15G9.4	0	13
X	egl-15	F58A3.2	0	20
X	ser-2	C02D4.2	0	20
X	nas-39	F38E9.2	0	21
X	gpn-1	F59D12.4	0	22